Hindawi
Advances in Civil Engineering
Volume 2018, Article ID 9249382, 12 pages
https://doi.org/10.1155/2018/9249382

Research Article

Temperature Control Measures and Temperature Stress of Mass Concrete during Construction Period in High-Altitude Regions

Zhenhong Wang,[1] **Li Tao**,[2] **Yi Liu**,[1] **and Jiang Yunhui**[1]

[1]*State Key Laboratory of Simulation and Regulation of Water Cycle in River Basin, China Institute of Water Resources and Hydropower Research, Beijing 100038, China*
[2]*Large Dam Safety Supervision Center, National Energy Administration, Hangzhou 311122, China*

Correspondence should be addressed to Zhenhong Wang; faithzhen@126.com

Received 13 August 2017; Accepted 25 June 2018; Published 26 July 2018

Academic Editor: Hugo Rodrigues

The focus on the development of China's vast hydropower resources has shifted to Tibet and other plateau regions. These areas are high-altitude regions whose basic climatic characteristics are as follows: dry climate, significant differences in daily temperature, and strong solar radiation. If a dam is built under such special climate conditions, specific and strict temperature control and crack prevention measures should be taken. Therefore, this study explores the temperature control standards, as well as temperature control and crack prevention measures, for concrete in high-altitude regions using three-dimensional finite element methods and based on the concrete gravity dam in Tibet in combination with the characteristics of material properties that are disadvantageous to temperature control and crack prevention. The temperature drop process can be optimized in time, and the temperature drop rate can be controlled to prevent excessive scale and temperature drop rates. Moreover, the temperature gradient can be spatially optimized, and thus, the differences in foundation temperatures, upper- and lower-layer temperatures, and internal and external temperatures can also be reduced. The research shows that the recommended temperature control and crack prevention measures can effectively reduce temperature stress. This study has a significant value as a reference for similar projects in high-altitude regions.

1. Introduction

The cracking of concrete dams has long been a highly common phenomenon [1]. Many scholars, both at home and abroad, have focused on solving the concrete crack problem for long term. Despite a series of achievements [2–8], completely preventing crack initiation during construction is difficult in view of the randomness and particularity of ambient temperature, the complexity of crack formation, the uncertainty of various factors in the construction process, the lack of in-depth understanding of concrete material characteristics, the insufficient safety margin of engineering design, and imperfect cause formation mechanisms [9–12]. This issue applies to both concrete and roller-compacted concrete dams. Therefore, the cracking problem should still be considered a key issue in dam construction.

The basic climatic characteristics in high-altitude regions are dry climates, significant differences in daily temperature, and strong solar radiation [13–16]. Hence, preventing crack formation in these areas is more difficult than constructing concrete dams in warm and humid low-altitude regions. Although a certain amount of temperature control and crack prevention experience has been accumulated in relation to dam construction in the relatively high-altitude regions of Sichuan [17], mature and strong systematic experience remains lacking. Therefore, the current study explores the temperature control standards, as well as temperature control and crack prevention measures, in concrete construction at high-altitude regions. It uses the three-dimensional finite element method and is based on one concrete gravity dam of Tibet (known as the Roof of the World) in combination with the mechanism and the causes

of dam general crack formation [18–24]. Furthermore, this study selects scientific, reasonable, and strong operational temperature control measures and methods to guide dam design and construction through the optimization, comparison, and analysis of schemes.

2. Simulating Calculation Principle

2.1. Calculation Principle of Temperature Field. At any point within concrete computational domain R, unstable temperature field T (x, y, z, and t) should satisfy the heat conduction continuity equation:

$$\frac{\partial T}{\partial t} = a\left(\frac{\partial^2 T}{\partial x^2} + \frac{\partial^2 T}{\partial y^2} + \frac{\partial^2 T}{\partial z^2}\right) + \frac{\partial \theta}{\partial \tau} \quad (\forall (x, y, z) \in R), \tag{1}$$

where T is the concrete temperature (°C), a is the thermal diffusivity (m^2/h), θ is the adiabatic temperature rise (°C), τ is the age (d), and t is the time (d).

By using variation principle, the solution of unstable temperature field differential control (1) is equivalent to the extreme problem of the functional $I(T)$ under the definite condition:

$$\begin{aligned} I(T) = {} & \iiint_R \left\{\frac{1}{2}\left[\left(\frac{\partial T}{\partial x}\right)^2 + \left(\frac{\partial T}{\partial y}\right)^2 + \left(\frac{\partial T}{\partial z}\right)^2\right] \right. \\ & \left. + \frac{1}{a}\left(\frac{\partial T}{\partial t} - \frac{\partial \theta}{\partial \tau}\right)T\right\} dx\, dy\, dz \\ & + \iint_{\Gamma^3} \frac{\beta}{\lambda}\left(\frac{T}{2} - T_a\right)T\, ds. \end{aligned} \tag{2}$$

If the domain R is dispersed by using finite element, the following can be obtained:

$$\begin{aligned} I(T) &= \sum_e I^e = \sum_e I_1^e + \sum_e I_2^e, \\ I_1^e &= \iiint_R \left\{\frac{1}{2}\left[\left(\frac{\partial T}{\partial x}\right)^2 + \left(\frac{\partial T}{\partial y}\right)^2 + \left(\frac{\partial T}{\partial z}\right)^2\right] \right. \\ &\quad \left. + \frac{1}{a}\left(\frac{\partial T}{\partial t} - \frac{\partial \theta}{\partial t}\right)T\right\} dx\, dy\, dz, \\ I_2^e &= \iint_{\Gamma^3} \frac{\beta}{\lambda}\left(\frac{T}{2} - T_a\right)T\, ds. \end{aligned} \tag{3}$$

In the finite element method calculation, the temperature interpolation equation at any point in each element is

$$T = \sum_{i=1}^{m} N_i T_i. \tag{4}$$

Replacing formula (4) into (2), the recursive equations solved for temperature field from the extreme condition $\delta I/\delta T = 0$ of functional are obtained; when the time coordinate uses the format of backward difference, there will be

$$\left([H] + \frac{1}{\Delta t_n}[R]\right)\{T_{n+1}\} - \frac{1}{\Delta t_n}[R]\{T_n\} + \{F_{n+1}\} = 0,$$

where $H_{ij} = \sum_e \left(h_{ij}^e + g_{ij}^e\right)$

$$R_{ij} = \sum_e r_{ij}^e,$$

$$F_i = \sum_e \left(-f_i^e - p_i^e\right)$$

$$\begin{aligned} h_{ij}^e &= \iiint_{\Delta R_i} \left(\frac{\partial N_i}{\partial x}\frac{\partial N_j}{\partial x} + \frac{\partial N_i}{\partial y}\frac{\partial N_j}{\partial y} + \frac{\partial N_i}{\partial z}\frac{\partial N_j}{\partial z}\right) dx\, dy\, dz \\ &= \int_{-1}^{1}\int_{-1}^{1}\int_{-1}^{1} \left(\frac{\partial N_i}{\partial x}\frac{\partial N_j}{\partial x} + \frac{\partial N_i}{\partial y}\frac{\partial N_j}{\partial y} + \frac{\partial N_i}{\partial z}\frac{\partial N_j}{\partial z}\right)|J|\, d\xi\, d\eta\, d\zeta, \end{aligned}$$

$$\begin{aligned} g_{ij}^e &= \frac{\beta}{\lambda}\iint_{\Delta S} N_i N_j\, dS \\ &= \frac{\beta}{\lambda}\int_{-1}^{1}\int_{-1}^{1} N_i N_j \sqrt{E_\eta E_\zeta - E_{\eta\zeta}^2}\Big|_{\xi=\pm 1} d\eta\, d\zeta \end{aligned}$$

$$\begin{aligned} r_{ij}^e &= \iiint_{\Delta R} \frac{1}{a} N_i N_j\, dx\, dy\, dz \\ &= \frac{1}{a}\int_{-1}^{1}\int_{-1}^{1}\int_{-1}^{1} N_i N_j |J|\, d\xi\, d\eta\, d\zeta, \end{aligned}$$

$$\begin{aligned} f_{ij}^e &= \iiint_{\Delta R} \frac{1}{a}\left(\frac{\partial \theta}{\partial \tau}\right)_{t_i} N_i\, dx\, dy\, dz \\ &= \frac{1}{a}\left(\frac{\partial \theta}{\partial \tau}\right)_{t_i}\int_{-1}^{1}\int_{-1}^{1}\int_{-1}^{1} N_i |J|\, d\xi\, d\eta\, d\zeta, \end{aligned}$$

$$p_{ij}^e = \frac{\beta}{\lambda}\iint_{\Delta S} T_a N_i\, dS = T_a \frac{\beta}{\lambda}\int_{-1}^{1}\int_{-1}^{1} N_i \sqrt{E_\eta E_\zeta - E_{\eta\zeta}^2}\Big|_{\xi=\pm 1} d\eta\, d\zeta. \tag{5}$$

If the temperature T_n at the previous moment is known, the temperature T_{n+1} at the next moment can be obtained.

2.2. Calculation Principle of Stress Field. The strain increment of the concrete under comprehensive stress state contains elastic strain increment, creep strain increment, temperature strain increment, dry shrinkage strain increment, and autogenic volume strain increment. Thus,

$$\{\Delta\varepsilon_n\} = \{\Delta\varepsilon_n^e\} + \{\Delta\varepsilon_n^c\} + \{\Delta\varepsilon_n^T\} + \{\Delta\varepsilon_n^s\} + \{\Delta\varepsilon_n^0\}, \tag{6}$$

where $\{\Delta\varepsilon_n^e\}$ is the concrete elastic strain increment, $\{\Delta\varepsilon_n^c\}$ is the creep strain increment, $\{\Delta\varepsilon_n^T\}$ is the temperature strain increment, $\{\Delta\varepsilon_n^s\}$ is the dry shrinkage strain increment, and $\{\Delta\varepsilon_n^0\}$ is the autogenic volume.

Table 1: Meteorological information on the gravity dam.

Item (°C)	January	February	March	April	May	June	July	August	September	October	November	December	Year
Mean annual temperature	0.3	2.9	6.5	9.7	13.3	16.4	16.6	16.1	14.4	10.4	4.7	0.7	9.3
Mean annual maximum temperature	10.6	12.4	15.7	18.5	21.9	24.7	24.4	23.6	22.3	19.9	15.2	11.5	18.4
Mean annual minimum temperature	−8.2	−5.6	−1.4	2.4	6.4	10.7	11.8	11.5	9.6	3.3	−3.1	−7.4	2.5
Extreme maximum temperature	23.4	24.0	32.0	28.8	30.8	31.8	32.5	30.3	29.2	27.1	24.8	21.0	32.5
Extreme minimum temperature	−16.6	−14.0	−10.0	−5.4	−3.3	2.0	4.4	4.9	0.7	−5.4	−10.5	−14.7	−16.6

Based on the physical equation, geometrical equation, and balance equation, the finite element governing equation on domain R_i at any time duration Δt_i can be obtained:

$$[K_i]\{\Delta\delta\}_i = \left\{\Delta P_i^G\right\} + \left\{\Delta P_i^C\right\} + \left\{\Delta P_i^T\right\} + \left\{\Delta P_i^S\right\} + \left\{\Delta P_i^0\right\}, \tag{7}$$

where $\{\Delta\delta_i\}$ is the displacement increment of all nodes in three directions within the concrete area R_i; $\{\Delta P_i^G\}$ is the equivalent node force increment caused by an external load within the time duration Δt_i, and it is the equivalent node force increment due to temperature change; $\{\Delta P_i^S\}$ is the equivalent node force increment resulting from dry shrinkage; and $\{\Delta P_i^0\}$ is the equivalent node force increment due to autogenic volume deformation.

By accumulating the displacement and stress increments, the displacement field and stress field of calculation domain at any moment can be obtained:

$$\begin{aligned} \delta_i &= \sum_{j=1}^{N} \Delta\delta_j, \\ \sigma_i &= \sum_{j=1}^{N} \Delta\sigma_j. \end{aligned} \tag{8}$$

2.3. Finite Element Method Calculation Program. The finite element calculation program (SAPTIS) used in this paper is a large-sized structural temperature, deformation, and stress analysis system [25, 26], including preprocessor, postprocessor, and analyzer. It can be used to not only simulate the change of temperature field and stress field in construction and operation of concrete structures but also simulate the impact of many factors and measures on temperature field and stress field during placing, including temperature control measures such as water pipe cooling, surface insulation, casting temperature, casting process, and surface watering; the impact of various engineering measures such as grouting, bolt and anchor cable, and foundation treatment on engineering structure deformation, stress, and bearing capacity and the simulation of opening and closing of many kinds of joints in the structure such as cross joints and cracks. This program has been applied in simulation and analysis of tens of middle- and large-sized projects at home and abroad as the Three Gorges, Xiaowan, Xiluodu, Longtan, Jinping, Guangzhou, Wudu, Xiangjiaba, Gong bazan in Pakistan, and so on.

3. General Situations of the Project and the Difficulty of Temperature Control and Crack Prevention

One hydropower station is located at the junction between Giacha County and Sangri County, Shannan Prefecture, Tibet Autonomous Region (TAR). The total length of the dam crest is 340 m, its elevation is 3378.0 m, the maximum height of the dam is 117.0 m, the maximum width of the dam base is 99.8 m, and the maximum width of the dam section is 32.5 m. The dam has also been divided into 14 sections. The results of the analysis and research on data obtained from the gravity dam show that this dam displays the following characteristics and difficulties:

(1) The basic climatic characteristics of this region is dry climate, cold winters and cool summers, significant differences in daily temperature, long low-temperature seasons, and strong solar radiation. This type climatic characteristic is disadvantageous to temperature control and crack prevention, and surface cracks are easily generated in concrete. The meteorological information on the gravity dam is shown in Table 1.

(2) The data on the mixture ratio of concrete indicate that the material properties adversely affect temperature control. The adiabatic temperature rise is high; its thermal expansion coefficient is great. Nonetheless, the modulus of elasticity and the ultimate tensile value or tensile strength of the gravity dam also does not have the advantage. Therefore, the difficulties of temperature control and crack prevention at this gravity dam should be large. The temperature control parameters of this and another dam in the same area are compared in Table 2.

Table 2: Comparison information on the temperature control parameters for the two gravity dams.

Project	Coefficient of thermal expansion ($10^{-6} \times {}^{\circ}C^{-1}$)	Adiabatic temperature rise of dam-body concrete (°C)	Self-grown volume deformation (120 days) (10^{-6})	Modulus of elasticity (90 days) (GPa)	Axial tensile strength (90 days) (MPa)	Ultimate tensile value (90 days) (10^{-4})
This gravity dam	9.0	26.3	−20.0	20.2	2.03	1.09
Another gravity dam	7.4	23.8	−19.9	20.2	2.14	1.12

Table 3: Temperature control schemes.

Temperature control measures for concrete			Scheme 1	Scheme 2	Scheme 3	Scheme 4
Pouring temperature (°C)	Strongly restrained zone		≤12	≤14	≤12	≤12
	Weakly restrained zone		≤13	≤15	≤13	≤13
	Unrestrained zone		≤14	≤16	≤14	≤14
Simultaneous cooling (m)	Initial stage of simultaneous cooling		Midphase	Midphase	Midphase + phase II	Midphase
	Height of the simultaneous cooling zone (m)		27	27	27 + 18	18
Spacing between water pipes (m)	Strongly restrained zone		1.5 × 1.5	1.5 × 1.5	1.5 × 1.5	1.5 × 1.5
	Weakly restrained zone		1.5 × 3.0	1.5 × 3.0	1.5 × 3.0	1.5 × 3.0
	Unrestrained zone		1.5 × 3.0	1.5 × 3.0	1.5 × 3.0	1.5 × 3.0
Pipe cooling	Phase I cooling	Water temperature (°C)	8.0	8.0	8.0	8.0
		Flow rate ($m^3 \cdot h^{-1}$)	1.5	1.5	1.5	1.5
		Initial flood period (day)	0.0	0.0	0.0	0.0
		Target temperature (°C)	19–20	19–20	19–20	19–20
	Midphase cooling	Water temperature (°C)	12	12	12	12
		Flow rate ($m^3 \cdot h^{-1}$)	0.8	0.8	0.8	0.8
		Initial flood period (day)	30–45	30–45	30–45	30–45
		Target temperature (°C)	16–18	16–18	16–18	16–18
	Phase II cooling	Water temperature (°C)	6–8	6–8	6–8	6–8
		Flow rate ($m^3 \cdot h^{-1}$)	1.0	1.0	1.0	1.0
		Initial flood period (day)	≥90	≥90	≥90	≥90
		Target temperature (°C)	10	10	10	10
Thickness of poured layers (m)	Strongly restrained zone		1.5	1.5	1.5	1.5
	Weakly restrained zone		3.0	3.0	3.0	3.0
	Unrestrained zone		3.0	3.0	3.0	3.0
Intermittent period (day)			10	10	10	10
Surface heat preservation			Yes	Yes	Yes	Yes

Note. (1) By the end of Phase I cooling, the temperature is controlled until midphase cooling begins. Once the target temperature in midphase cooling is reached, the temperature is controlled until Phase II cooling is initiated. (2) The temperature drop rate of Phase I cooling is less than $0.5^{\circ}C \cdot day^{-1}$, whereas that of midphase cooling is less than $0.3^{\circ}C \cdot day^{-1}$. (3) When the concrete is poured in winter, the pouring temperature should be greater than 6°C. (4) The midphase + Phase II scheme suggests that simultaneous cooling height of 27 m begins in midphase, whereas that height of 18 m starts in Phase II.

4. Temperature Control and Crack Prevention Scheme Optimization

As the main method to reduce temperature stress under adverse environmental and climatic conditions and with concrete materials, the differences in the foundation temperatures, upper- and lower-layer temperatures, and internal and external temperatures of the gravity dam should be controlled. The difference in foundation temperatures refers to the variation in the maximum temperature of concrete and in the stable temperature of the dam. The difference in the upper- and lower-layer temperatures is the temperature difference among the layers of poured concrete. The difference in internal and external temperatures refers to the variation between the internal and surface temperatures of concrete. As long as these temperature differences are controlled, concrete deformation can be controlled as well; that is, the mutual restraint and temperature stress among concretes can be reduced. Therefore, this study mainly focuses on three principles, namely, accurately determining the stable temperature field of the dam, temporally optimizing temperature control measures, and spatially optimizing these measures.

Based on these three principles, the following overall temperature control concept for the gravity dam is proposed: (1) temperature control standards and measures are developed in terms of spatial elevation in accordance with strongly restrained, weakly restrained, and free zones; (2) the control of the difference in foundation temperatures at the strongly restrained zone is strengthened; (3) the control of the temperature gradient is enhanced; (4) the pouring and maximum temperatures are reduced; and (5) the surface

Table 4: Mixing proportion of dam concrete.

Design indexes	Main parameters of mixing proportion						
	Sand percentage (%)	Water-binder ratio	Water consumption (kg/m^3)	FA dosage (%)	Water-reducing agent (%)	Air-entraining agent (10,000)	Volume weight (kg/m^3)
Dam concrete C9020W6F100	24	0.55	85	35	0.8	2.0	2410

Table 5: Main thermodynamic parameters of dam concrete.

Name of index	Unit	Dam concrete
Thermal diffusivity	10–3 m^2/h	2.82
Coefficient of thermal conductivity	kJ/(m·h·°C)	6.12
Specific heat	kJ/(kg°C)	0.90
Coefficient of linear expansion	10–6/°C	9.00
Volume weight	kN/m^3	24.10
Poisson's ratio	—	0.17

protection is protected effectively. In addition, the differences in internal and external temperatures are reduced. In line with this concept, four temperature control schemes are developed, and the difference of these schemes is mainly shown in the pouring temperature and the height of the simultaneous cooling zone, as depicted in Table 3.

4.1. Mixing Proportion of Concrete and Parametric Model. For mixing proportion of concrete in the dam, refer Table 4. The aggregate used mainly is biotite granodiorite. Table 5 lists the thermodynamic parameters of the concrete. It can be seen from the table that the coefficient of thermal expansion of the concrete is slightly big, which has adverse impact on the temperature control and crack prevention. The adiabatic temperature rise and elastic modulus are two most important thermodynamic parameters. Equations (9) and (10) are the calculation parameter model used when carrying out simulating calculation:

$$\text{Adiabatic temperature rise model } \theta(\tau) = 26.26 \times \frac{\tau}{(3.73+\tau)}, \tag{9}$$

$$\text{Elastic modulus model } E(\tau) = 28.6 \times \left(1 - e^{-0.33\times\tau^{0.334}}\right). \tag{10}$$

4.2. Computational Model and Boundary Conditions. 3D finite element method is used for simulating calculation, the number of computational model units is 60,744, the number of nodes is 71,049, and it mainly includes the dam itself and a certain range of foundation under the dam. The temperature gradient of concrete surface is relatively bigger due to contact with air temperature or water temperature; therefore, the division of the grids is relatively finer, the inside grids are worse, and the spatial hexahedron isoparametric element is used when dividing the grid.

When calculating the temperature field, the upstream and downstream faces of the dam are the third kind of boundary; by taking into consideration the local temperature and solar radiation, they will be the first kind of boundary after impounding, that is, the water temperature of the reservoir with corresponding elevation; as the actual foundation is infinitely great, it should be taken into consideration that the surrounding and bottom of the foundation model is adiabatic boundary when carrying out calculation, the upper surface is the third kind of boundary condition, and the air temperature and solar radiation should be taken into consideration.

When carrying out the calculation, by combining the actual condition of the project, the bottom of the foundation is a three-dimensional constraint, the surrounding of the foundation is a normal constraint, and the boundary surface of other structures are free deformation surface. For 3D finite element computational model, refer Figure 1; the boundary conditions of model calculation are as shown in Figures 2(a) and 2(b).

4.3. Stable Temperature Field of a Dam. The stable temperature field refers to the final temperature reached under the influence of the external environment after concrete hydration. The stable temperature field is considered an important basis by which the following can be determined: the maximum temperature of concrete, pouring temperature, the allowable temperature difference in the foundation, joint grouting temperature, and the necessary preconditions for the development of temperature control measures. As mentioned previously, the gravity dam is located in the high-altitude region of Tibet (the Roof of the World) and has the following basic climatic characteristics: a mean annual air temperature of 9.3°C, an average annual water temperature of 9.8°C, and an average annual ground temperature of 10.3°C. The stable temperature of the gravity dam is therefore set as 10°C based on three-dimensional calculations and on a comprehensive consideration of these influencing factors.

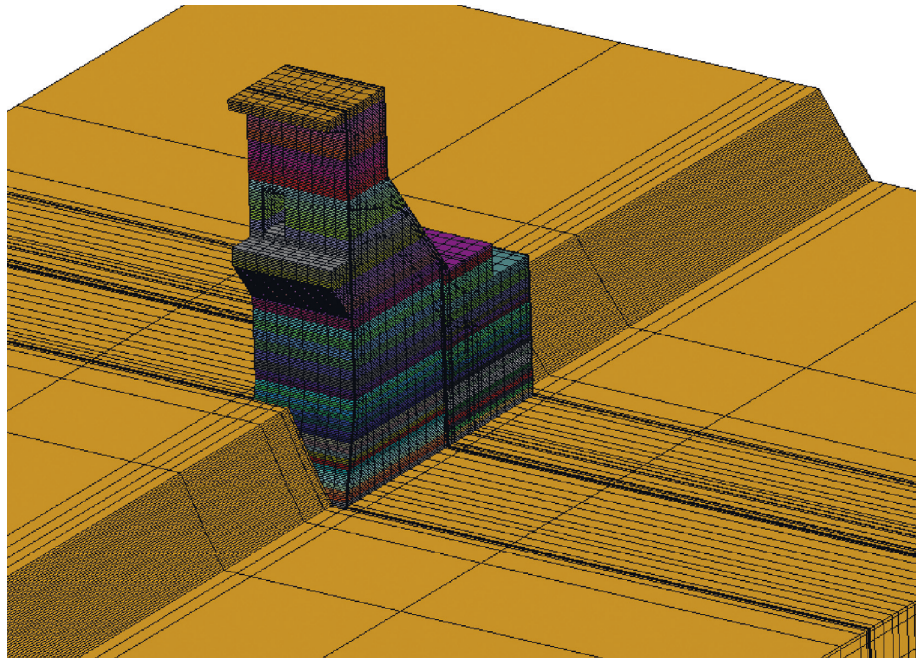

Figure 1: 3D finite element computational model.

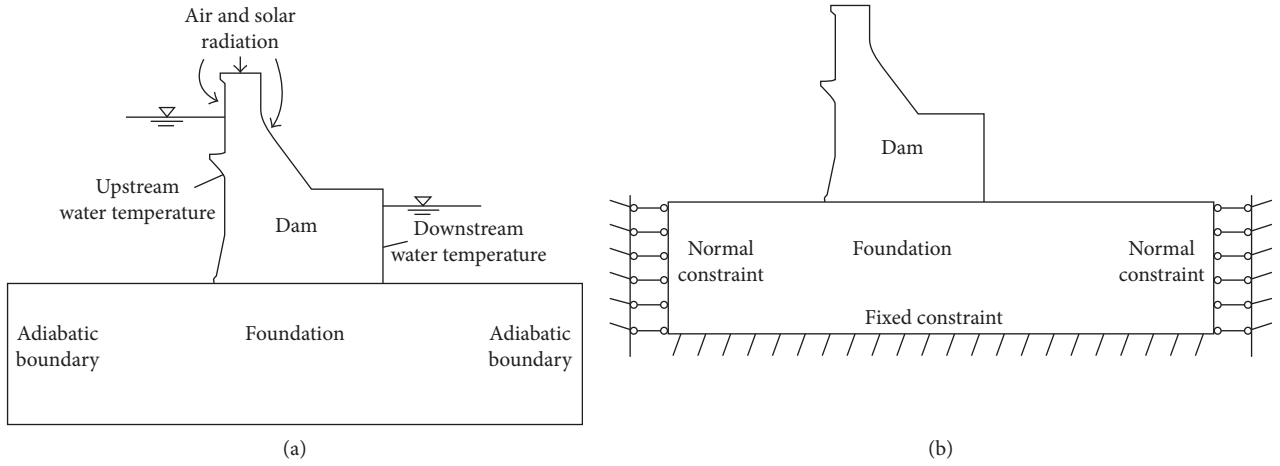

Figure 2: Boundary conditions of computational model: (a) temperature boundary conditions; (b) stress boundary conditions.

4.4. Temporal Optimization of Temperature Control Measures for Dam. To optimize temperature control measures, the temperature variation of concrete should mainly be controlled in time or during the process of concrete hardening development so that the concrete can be developed according to the set temperature variation process. This set process can meet anticracking requirements as an ideal temperature development process because of the reduced stress and the increased safety coefficient of concrete. The measures for heat preservation can be implemented to limit the difference between the internal and external temperatures of concrete and to reduce the effect of ambient temperature variation in the vicinity of the concrete. The measures for water pipes can reduce the internal temperature to limit the differences in foundation temperatures and in the internal and external temperatures. The cooling process can also been divided into three cooling phases. Each phase has a different water temperature, flow rate, and cooling rate to meet the needs of the ideal cooling process. It can be seen from Figure 3 that the temperature change process of concrete is strictly controlled. It is divided into three stages, and each stage has a strict requirement of the target temperature and cooling rate, which realizes the slow cooling of concrete, ensures the smaller temperature gradient on the time change, and prevents the cracks from producing.

4.5. Spatial Optimization of the Temperature Control Measures for a Dam. To spatially optimize temperature control measures, the temperature variation of concrete can primarily be controlled in a structure space, especially that of

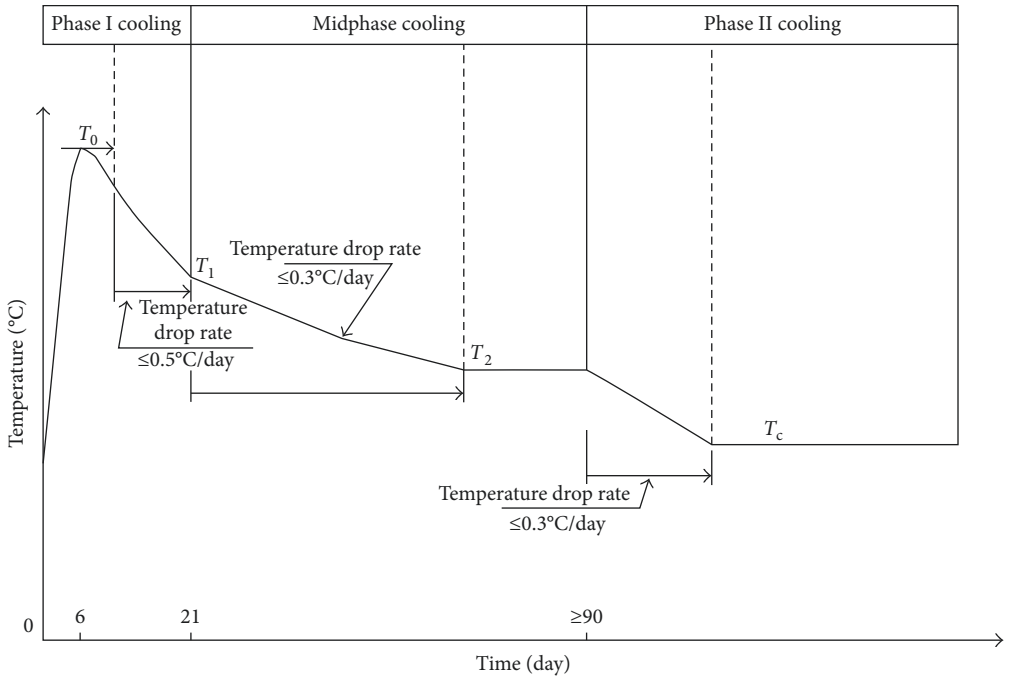

Figure 3: The control process of concrete temperature change.

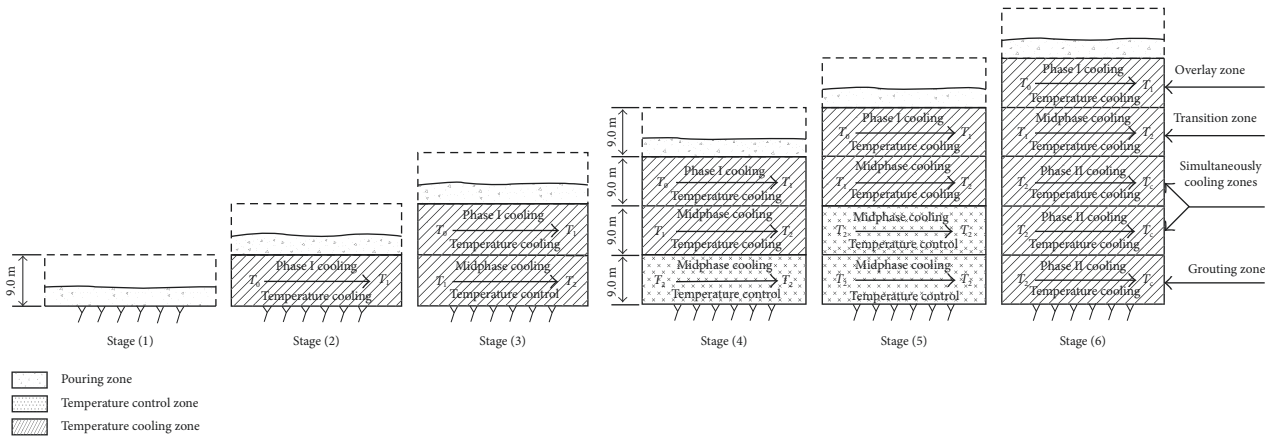

Figure 4: The formation of temperature gradient in concrete space and its corresponding temperature control process: (1) maximum elevation of the grouting subzone at the dam is 9 m; that is, a grout compartment is set every 9 m; (2) grouting zone: one grout compartment in which the longitudinal joints are grouted; (3) simultaneous cooling zone: when the grouting zone is located at the first grout compartment at the bottom of the restrained zone, the simultaneous cooling zone should consist of two grout compartments on top of the grouting zone. The other section should consist of one grout compartment on top of the grouting zone; (4) transition zone: one grout compartment on top of the simultaneous cooling zone; and (5) overlay zone: one grout compartment on top of the transition zone. (6) With the placement of concrete, four zones are gradually formed in the high direction. When the lowest area has reached the target temperature of the grouting zone, the four zones above are simultaneous cooling zones, transition zone, and overlay zone. Through the simultaneous cooling of the four regions, the mutual restraint and temperature stress are reduced.

concrete at the foundation restrained zone and of the concrete poured in high-temperature seasons. This control limits the constraint induced by the foundation and the upper and lower layers to reduce temperature stress. (1) Reduction of the pouring temperature at the foundation restrained zone, the encryption of the cooling water pipe, the control of maximum temperature, and the limitation of the difference in foundation temperatures. (2) The setup of the simultaneous cooling zone and the reduction of the difference in the upper- and lower-layer temperatures. It can

Table 6: Calculated results of temperature and stress according to the schemes.

Operating condition	Maximum temperature of the strongly restrained zone (°C)	Maximum tensile stress of the strongly restrained zone		
		σ_x (MPa)	Elevation (m)	Safety coefficient k
Scheme 1	27.54	1.40	3264.5	1.81
Scheme 2	28.72	1.45	3264.5	1.74
Scheme 3	27.54	1.48	3264.5	1.71
Scheme 4	27.54	1.49	3264.5	1.70

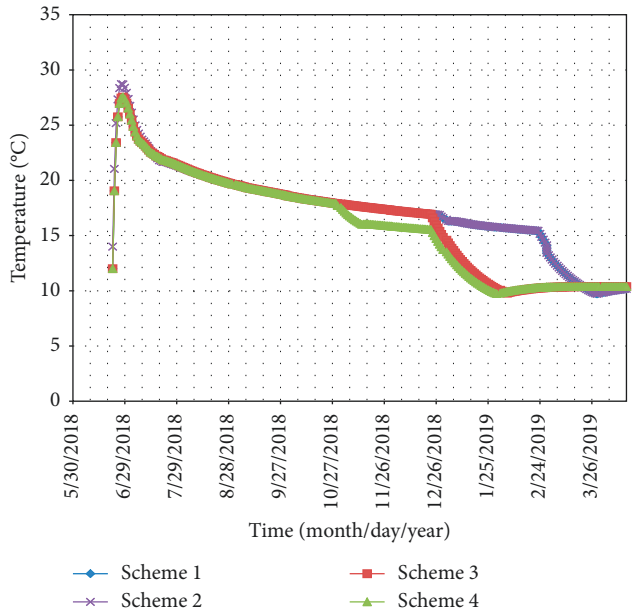

Figure 5: Temperature/process time curves of typical characteristic points according to the different schemes.

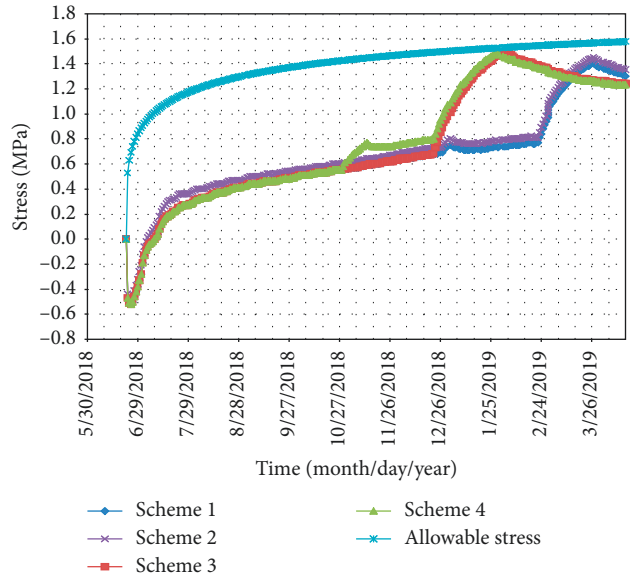

Figure 6: Stress/process time curves of typical characteristic points according to the different schemes.

be seen from Figure 4 that, with the concrete pouring in a high direction, the cooling process of each layer is coordinated by controlling the cooling mode of each layer, and then the temperature gradient of concrete in the high direction is controlled, the mutual restraint of concrete is reduced, and finally, the risk of cracking is reduced.

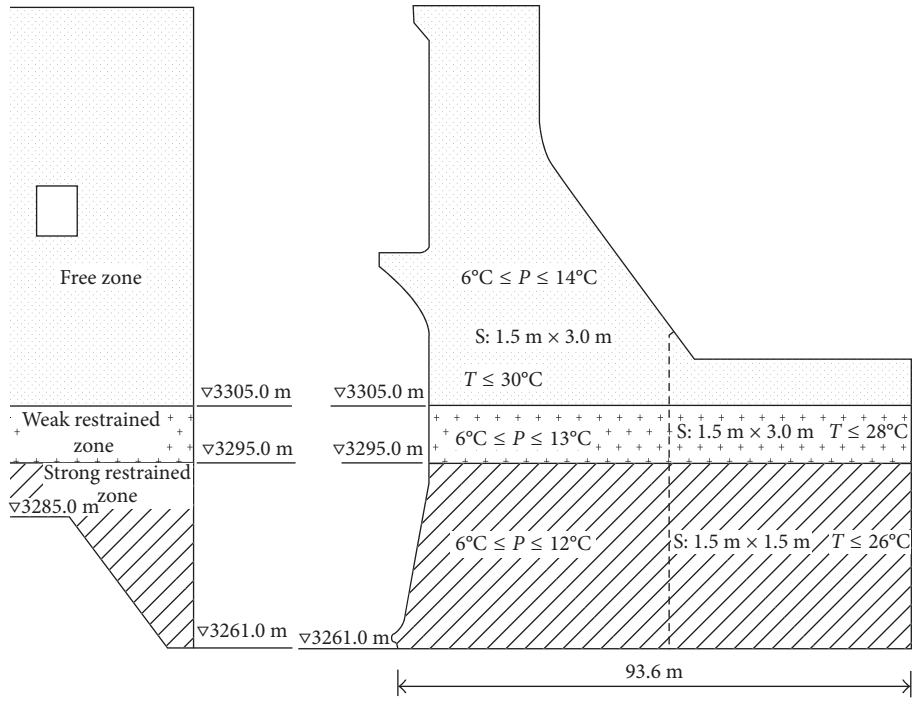

Figure 7: Distribution diagram of the basic conditions and temperature control measures for dam: (a) distribution of the basic temperature control measures and (b) cooling mode (the lower three grouting zones should be cooled simultaneously).

4.6. Comparison of the Effects of Different Temperature Control Measures. The temperature control measures can be optimized temporally to induce significant effects. The calculated results indicate that the temperature of concrete can change stably under three-stage water pipe cooling conditions, thus preventing the early stress from exceeding the standard as a rapid temperature drop. Moreover, the excessive stress induced by the significant temperature drop later on in the process can be avoided. Given strong Phase I and midphase cooling effects, Phase II cooling time should be appropriately delayed to forestall the onset of maximum stress, to emphasize the creep effect of concrete, and to reduce the stress experienced later on in the process (from 1.49 MPa to 1.40 MPa). At the same time, the strength of concrete increases continuously; correspondingly, the safety coefficient of concrete increases significantly as well (from 1.70 to 1.81 as shown in Table 6 and Figure 5).

Temperature control measures can be optimized as per spatial distribution to reduce stress significantly. According to the calculated results (Figure 6), the following can be obtained: (1) the maximum height of the simultaneous cooling zone is 27 m, and the three grouting zones can be cooled simultaneously starting from midphase cooling. Furthermore, the restriction on the concrete is relatively minimal given the small temperature difference between the upper and lower grouting zones and the synchronous deformation. The maximum stress reaches 1.40 MPa. (2) The height of the simultaneous cooling zone reaches 18 m starting from Phase II cooling. The maximum stress of the strongly restrained zone increases to 1.48 MPa. (3) If the height of the simultaneous cooling zone reaches 18 m and the temperature drops starting from midphase cooling, then the maximum stress is 1.49 MPa. Scheme 1 and Scheme 3 are significantly better than Scheme 2.

Based on the spatial-temporal optimization of temperature control measures, the pouring temperature can be decreased to reduce the maximum temperature. Therefore, the pouring temperature should be lowered under allowable engineering conditions to manage temperature effectively and to prevent crack formation (comparison of Schemes 1 and 2).

In conclusion, the height of the simultaneous cooling zone can significantly affect concrete stress, especially the first and second grout compartments of the strongly restrained zone. Therefore, this height should be increased as much as possible to reduce the stress in Phase II cooling.

5. Recommended Temperature Control Measures and Standards

Therefore, the temperature control of Scheme 1, as well as its crack prevention measures and standards, should be applied based on the numerical comparison of the schemes in combination with the lessons gained from experiences with similar built-up projects in the same region. That is, the stable temperature field should be 10°C, the maximum allowable temperature of concrete at the strongly restrained zone should be 27.5°C, the allowable difference in foundation temperature should be 17.5°C, and the three-phase cooling method should be used during concrete cooling. Moreover, the cooling process can be optimized temporally. The concrete at the strongly restrained zone can also be cooled using the simultaneous cooling method of the three grouting zones starting from midphase, and the temperature distribution can be optimized spatially. The recommended distribution diagram of the basic conditions and temperature control measures for the dam is depicted in Figure 7.

It can be seen from Figure 7 that the temperature control standard is set to be the strongly restrained zone, the weak constraint zone, and the free zone in the height direction of the dam. The standard of the strongly restrained zone is the very strict, and the free zone is relatively loose (Figure 7(a)). For the cooling measures of concrete, it is carried out according to the simultaneous cooling method to reduce the mutual restraint between the pouring layers. Then, the risk of cracking can been reduced (Figure 7(b)).

6. Conclusions

(1) Implementing temperature control and crack prevention measures for concrete dams is difficult given the basic climatic characteristics of Tibetan high-altitude regions. Moreover, the size, body type, and structure of the dam are similar to those of another dam, but the material properties of dam concrete are quite different from those of another dam concrete. Although the elastic modulus parameters are moderate, adiabatic temperature rise and thermal expansion coefficient are relatively large. Thus, the material parameters of the dam concrete are disadvantageous for anticracking measures.

(2) Based on the research results, temperature should be controlled during construction according to the principles of "early thermal insulation, small temperature difference, and slow cooling." Moreover, temperature control measures should be spatially and temporally optimized. The differences in foundation temperatures, upper- and lower-layer temperatures, and internal and external temperatures should be reduced as well. The temperature control measures and standards for strongly restrained zones should be strengthened.

(3) An intelligent water supply system can help facilitate the rationalization and optimization of the drop process of temperature. According to the temperature measured in real time, the required flow can be fed back, calculated, and adjusted to facilitate automatic intervention in cooling water supply. As a result, temperature will be effectively controlled. Thus, the implementation of intelligent water supply and cooling measures is recommended for the dam during construction.

Notations

t: Time (d)
R: Concrete computational domain
T: Concrete temperature (°C)

T (x, y, z, and t): Unstable temperature field
a: Thermal diffusivity (m^2/h)
θ: Adiabatic temperature rise (°C)
τ: Age (d)
$\{\Delta\varepsilon_n^e\}$: Concrete elastic strain increment
$\{\Delta\varepsilon_n^c\}$: Creep strain increment
$\{\Delta\varepsilon_n^T\}$: Temperature strain increment
$\{\Delta\varepsilon_n^s\}$: Dry shrinkage strain increment
$\{\Delta\varepsilon_n^0\}$: Autogenic volume
Δt_i: Any time duration
$\{\Delta\delta_i\}$: Displacement increment of all nodes in three directions within concrete area Ri
$\{\Delta P_i^G\}$: Equivalent node force increment caused by an external load within the time duration Δt_i
$\{\Delta P_i^S\}$: Equivalent node force increment resulting from dry shrinkage
$\{\Delta P_i^0\}$: Equivalent node force increment due to autogenic volume deformation
$\delta_i = \sum_{j=1}^{N} \Delta\delta_j$: Displacement field of calculation domain at any moment
$\sigma_i = \sum_{j=1}^{N} \Delta\sigma_j$: Stress field of calculation domain at any moment.

Conflicts of Interest

The authors declare that they have no conflicts of interest.

Acknowledgments

Wang Zhenhong acknowledges the support provided by the National Natural Science Foundation of China (Grant no. 51579252), the National Basic Research Program of China (973 Program 2013CB036406 and 2013CB032904), the Thirteenth Five-Year Plan for Science and Technology Support Project (2016YFC0401600), IWHR, and the Basin Water Cycle Simulation and Regulation of State Key Laboratory Special Research Foundation.

References

[1] D. Baoying, W. Guobing, and H. Shuping, "A review on causes of cracking in domestic concrete dams and preventive measures," *Water Resources and Hydropower Engineering*, vol. 4, pp. 12–18, 1994.

[2] W. Zhenhong, Z. Guoxin, and L. Yi, "Study on the application of cooling pipe in thin-walled concrete structure," in *Proceedings of International Conference on Structures and Building Materials*, pp. 1107–1110, Ghuangzhou, China, January 2011.

[3] A. Abdulrazeg, J. Noorzaei, M. Jaafar, P. Khanehzaei, and T Mohamed, "Thermal and structural analysis of RCC double-curvature arch dam," *Journal of Civil Engineering and Management*, vol. 20, no. 3, pp. 434–445, 2014.

[4] W. Zhenhong, Z. Yueming, and Y. Shuping, "Study on temperature control and crack prevention of thin-walled concrete structures during construction period," *Journal of Xi'an University of Architecture and Technology*, vol. 39, no. 6, pp. 773–778, 2007.

[5] W. Zhenhong, L. Yi, Z. Xin, and W. Hou, "Schematic study on temperature control and crack prevention during spillway tunnel concreting period," *Materials and Structures*, vol. 48, no. 11, pp. 3517–3525, 2015.

[6] W. Zhenhong, Z. guoxin, L. Yi, and Y. Shuping, "Sensitivity analysis of temperature control parameters and study on simultaneous cooling zone during dam constructions in high altitude regions," *Mathematical Problems in Engineering*, vol. 2015, Article ID 528589, 12 pages, 2015.

[7] W. Zhenhong, L. Yi, and Y. Shuping, "Surface thermal insulation and pipe cooling of spillways during concrete construction period," *Mathematical Problems in Engineering*, vol. 2014, Article ID 973680, 7 pages, 2014.

[8] Z. Zhiming, G. Xingwen, and D. Rongqiang, "Analysis of hydration heat-induced stresses and cracks in massive concrete walls," *Journal of Hohai University*, vol. 30, no. 5, pp. 12–16, 2002.

[9] A. K. Schindler and A. Karel, *Concrete Hydration, Temperature Development, and Setting At Early-Ages*, The University of Texas at Austin, Austin, TX, USA, 2002.

[10] A. Saetta, R. Scotta, and R. Vitaliani, "Stress analysis of concrete structures subjected to variable thermal loads," *Journal of Structural Engineering*, vol. 121, no. 3, pp. 446–457, 1991.

[11] D. Lelièvre, V. Nicolas, and P. Glouannec, "Numerical modeling of heat and mass transfer in porous materials during drying and shrinkage," in *COMSOL Conference*, Boston, UK, 2012.

[12] S. Tsimas and A. Moutsatsou-Tsima, "High-calcium fly ash as the fourth constituent in concrete: problems, solutions and perspectives," *Cement and Concrete Composites*, vol. 27, no. 2, pp. 231–237, 2005.

[13] M. Xueqiang, "Technical characteristics of water conservancy and hydropower construction in high-altitude regions," *Water Resources and Hydropower Engineering*, vol. 37, no. 7, pp. 45–49, 2006.

[14] L. Lianxin, "Study on high-performance concrete and its technologies in high-altitude & Alpine regions," *Construction Technologies*, vol. 34, no. S2, pp. 99–101, 2005.

[15] D. Ting, Z. Dengmin, and W. Yanhu, "Application of concrete construction technologies for Tibetan straight-hole hydropower station in the Alpine region at the low-temperature season," *Water Resources and Hydropower Engineering*, vol. 36, no. 7, pp. 106–108, 2005.

[16] S. Zhantao, Z. Yueming, Q. Sheng et al., "Study on temperature control and crack prevention of concrete gravity dam in the Alpine region," *Journal of Three Gorges University*, vol. 30, no. 1, pp. 6–8, 2008.

[17] Y. Hu, Z. Zuo, Q. Li, and Y. Duan, "Boolean-based surface procedure for the external heat transfer analysis of dams during construction," *Mathematical Problems in Engineering*, vol. 2013, Article ID 175616, 17 pages, 2013.

[18] F. L. Zhu, "Modeling heat and moisture transfer within porous textiles under high temperature gradients," *Advanced Materials Research*, vol. 455, pp. 1136–1139, 2012.

[19] D. Santillán, E. Salete, D. J. Vicente, and M. Á. Toledo, "Treatment of solar radiation by spatial and temporal discretization for modeling the thermal response of arch dams," *Journal of Engineering Mechanics*, vol. 140, no. 11, p. 05014001, 2014.

[20] Z. P. Bažant and S. Baweja, "Justification and refinements of model B3 for concrete creep and shrinkage 1. statistics and sensitivity," *RILEM Materials and Structures*, vol. 28, no. 7, pp. 357–365, 1995.

[21] M. Cervera, J. Oliver, and T. Prato, "Simulation of construction of RCC dams. I: temperature and aging," *Journal of Structural Engineering*, vol. 126, no. 9, pp. 1053–1060, 2000.

[22] G. de Schutter and L. Taerwe, "General hydration model for Portland cement and blast furnace slag cement," *Cement and Concrete Research*, vol. 25, no. 3, pp. 593–604, 1995.

[23] Y. Lee, M.-S. Choi, S.-T. Yi, and J.-K. Kim, "Experimental study on the convective heat transfer coefficient of early-age concrete," *Cement and Concrete Composites*, vol. 31, no. 1, pp. 60–71, 2009.

[24] G. De Schutter, "Finite element simulation of thermal cracking in massive hardening concrete elements using degree of hydration based material laws," *Computers and Structures*, vol. 80, pp. 2035–2042, 2002.

[25] Z. Guoxin, "Development and application of SAPTIS-a software of multi-field simulation and nonlinear analysis of complex structures (Part I)," *Water Resources and Hydropower Engineering*, vol. 1, pp. 31–36, 2013.

[26] L. Youzhi, Z. Guoxin, and Y. Ping, "Development and application of SAPTIS-a software of multi-field simulation and nonlinear analysis of complex structures (Part IV)," *Water Resources and Hydropower Engineering*, vol. 45, no. 8, pp. 33–37, 2014.